Environ Earth Sci (2010) 60:1509–1521
DOI 10.1007/s12665-009-0286-z

ORIGINAL ARTICLE

Landsat data to evaluate urban expansion and determine land use/land cover changes in Penang Island, Malaysia

Kok Chooi Tan · Hwee San Lim · Mohd Zubir MatJafri · Khiruddin Abdullah

Received: 5 July 2009 / Accepted: 17 August 2009 / Published online: 11 September 2009

Abstract Land surface temperature (LST) plays an important role in local, regional and global climate studies. LST controls the distribution of the budget for radiation heat between the atmosphere and the earth's surface. Therefore, it is important to evaluate abrupt changes in land use/land cover (LULC). Penang Island, Malaysia has been experiencing a rapid and drastic change in urban expansion over the past two decades due to growth in industrial and residential areas. The aim of this study was to investigate and evaluate the impact of LST with respect to land use changes in Penang Island, Malaysia. Three supervised classification techniques known as maximum likelihood, minimum distance-to-mean and parallelepiped were applied to the images to extract thematic information from the acquired scene by using PCI Geomatica 10.1 image processing software. These remote sensing classification techniques help to examine land-use changes in Penang Island using multi-temporal Landsat data for the period of 1999–2007. Training sites were selected within each scene and seven land cover classes were assigned to each classifier. The relative performance of each technique was evaluated. The accuracy of each classification map was assessed using a reference data set consisting of a large number of samples collected per category. Two Landsat satellite images captured in 1999 and 2007 were chosen to classify the LULC types using the maximum likelihood classification method, determined from visible and near-infrared bands. The study revealed that the maximum likelihood classifier produced superior results and achieved a high degree of accuracy. The LST and normalised difference vegetation index (NDVI) were computed based on changes in LULC. The results showed that the urban (highly built-up) area increased dramatically, and grassland area increased moderately. Inversely, barren land decreased obviously, and forest area decreased moderately. While urban (minimally built-up) area decreased slightly. These changes in LULC caused at significant difference in LST between urban and rural areas. Strong correlation values were observed between LST and NDVI for all LULC classes. The remote sensing technique used in this study was found to be efficient; it reduced the time for the analysis of the urban expansion, and it was found to be a useful tool to evaluate the impact of urbanisation with LST.

Keywords LST · LULC · Landsat · NDVI

K. C. Tan (✉) · H. S. Lim · M. Z. MatJafri · K. Abdullah
School of Physics, Universiti Sains Malaysia,
11800 Penang, Malaysia
e-mail: kokchooi86@gmail.com

H. S. Lim
e-mail: hslim@usm.my

M. Z. MatJafri
e-mail: mjafri@usm.my

K. Abdullah
e-mail: khirudd@usm.my

Introduction

Satellite images have been widely used to analyse temporal changes in land use/land cover (LULC) in Malaysia. However, only a few studies focused on the multi-temporal LULC over a small coverage area like Penang Island, Malaysia. The Landsat programme has provided invaluable information through the Landsat 7 ETM+ and Landsat 5 TM satellite images for the past few decades (Cohen and Goward 2004). Indeed, Landsat data are useful for monitoring land cover and vegetation density, because they are available in multi-spectral, multi-resolution and multi-

temporal forms and provide important information for analysis (Weng 2001).

Abrupt environmental changes in local, regional and global scales have become dangerous and threatening for humans in this century. Global environmental studies have increasingly been carried out over the past two decades (Houghton et al. 2001). Human activities, rather than natural forces, are the major causes of abrupt global environmental change. Anthropogenic activities have been proven to alter the global climate. This issue has caused concern, as adaptation to and mitigation of climate change can help to protect those most vulnerable to climate change. Changes in LULC and anthropogenic activities are the most obvious results of human modification of vegetation surfaces to impervious surfaces (Xiao and Weng 2007; Weng and Lo 2001). Studies of history of LULC changes in our study area help to evaluate the degree of human-induced environmental changes and the changes themselves.

Urbanisation has been a major type of land use and land cover change in human history (Weng 2001). Urbanisation is caused by the conversion of other types of land due to the growth of populations and economy. Improper planning and management of land use and land cover changes associated with urbanisation can have a great impact on the climate and local environment. For the past few decades, many researchers have focused on urbanisation and its impact on local regions. Generally, urban areas have a higher thermal conductivity and radiation heat budget. Therefore, by changing the vegetation, the land becomes more impervious, with road, buildings, concrete, etc. Due to the modification of the terrestrial ecosystem, urban areas tend to experience higher surface temperatures when compared to rural areas. These changes alter the solar heat radiation, surface temperature and heat storage in urban areas. Finally, the temperature difference between urban and rural areas contributes to the development of the urban heat island (UHI).

Land surface temperature (LST), which is a useful tool to predict radiation budgets for heat balance, plays an important role in human–environment interactions (Mallick et al. 2008). LST is an important factor controlling the chemical, physical and biological processes of earth systems (Liu et al. 2006). There are two methods used to compute LST: direct measurements taken on the ground and satellite-retrieved LST measurements. Satellite-retrieved LST data have a high spatial resolution and high coverage area and are less time-consuming when compared to ground measurement data. However, the retrieved LST value must be validated using ground truth measurement data. Furthermore, the validated data only apply to a flat, large and homogeneous coverage area in order to avoid uncertainty due to heterogeneity (Synder et al. 1997). To improve the accuracy of the satellite-retrieved LST, several factors must be considered by using image processing software or retrieval algorithms. These factors include the digital elevation, emissivity and atmospheric effects (Qin and Karnieli 1999; Han et al. 2004; Dash et al. 2002).

Study area

The study area, Penang Island, is located in the northern part of Malaysia, within latitudes 5°12′N to 5°30′N and longitudes 100°09′E to 100°26′E (Fig. 1). George Town, the second largest city in Malaysia and also the capital city in Penang state, is located in the east region of Penang Island. The area of Penang Island is approximately 295 km^2, and it is also the most populated island in the country, with an estimated population of 720,000.

Penang Island enjoys an equatorial climate throughout the entire year, which is warm and sunny. The average annual temperature varies between 27 and 30°C. The average mean daily temperature is about 27°C, and the mean daily maximum and minimum temperatures range between 31.4 and 23.5°C, respectively. The average annual relative humidity is between 70 and 90%, and the mean daily humidity varies between 60.9 and 96.8%. The average annual rainfall is about 267 cm, though the annual total can be as high as 624 cm (Ahmad et al. 2006). During periods of monsoon winds, the population can expect mostly sunshine during the day but rainfall in the evenings.

Fig. 1 The geographical features of the study area

The wettest periods are generally between April and May and October and November. Penang Island is generally free from environmental hazards and natural disasters. This makes it suitable for tourism year round. However, in 2004, Penang Island was hit by the Acheh tsunami. After this incident, the local authorities implemented a tsunami warning system along the beaches to help protect the residents and visitors from any hazards.

Recently, George Town was added to the UNESCO World Heritage List, indicating that George Town constitutes a unique architectural and cultural townscape in Southeast Asia. Hopefully, this recognition will help to increase the number of visitors at Penang Island and improve tourism in all of Malaysia. The Penang Heritage Trust, a non-governmental organisation, was formed to conduct a series of site visits to offer visitors a glimpse of the early development of George Town.

Penang Island is composed predominantly of hilly terrain, with the highest point being Western Hill (part of Penang Hill) at 830 m above sea level. The terrain consists of coastal plains, hills and mountains. The coastal plains are narrow, the most extensive of which are located in the northeast and forms a triangular promontory where George Town, is located. The topography of Seberang Perai is mostly flat. Butterworth, the main town in Seberang Perai, lies along the "Perai" River estuary and faces George Town at a distance of 3 km (2 miles) across the channel to the east (Penang-Wikipedia 2009, http://en.wikipedia.org/wiki/Penang).

Remotely sensed data

Two Landsat images, acquired on December 27, 1999 (Landsat 7 ETM+) and February 8, 2007 (Landsat 5 TM), were obtained for the study. The satellite images were chosen due to the following criteria (Sun et al. 2008): (1) the satellite images must have <10% cloud coverage over the total study area or be cloud-free if possible; (2) the satellite images should be available for a long time series, to maximise the separability and differentiate the different land use classes. Because Penang Island is located in the equatorial region, it is impossible to get 100% cloud-free data. However, both of the satellite images are covered by 10% clouds within the study area. The study areas are entirely contained within path 128, and row, 56.

Methodology

Image pre-processing

Multi-temporal images must be co-registered in the same coordinate system (e.g. UTM/WSG84) to detect changes in LST and land-cover (Chen et al. 2006). The change detection technique used here for LULC is based on a pixel-by-pixel analysis. The RMSE (root mean-square error) will be a good indicator to justify the accuracy of the co-registered images. Usually for Landsat images, the value for RMSE should not be >0.5 pixels (Lunetta and Elvidge 1998). A value of >1 pixel leads to a misinterpretation of LULC at the same point using multi-temporal images (Sun et al. 2008). With the aid of PCI Geomatica version 10.1, a digital image processing software, both satellite images were resampled to 25-m pixel size. Then, they were georectified using a second-order polynomial equation using the nearest neighbour method. Overall, RMS errors of <0.5 pixels were achieved in this study (Vicente-Serrano et al. 2008; Schroeder et al. 2006; Kabbara et al. 2008). Finally, the satellite image (acquired on December 27, 1999) was corrected to remove atmospheric effects by using a simple atmospheric correction method known as the darkest pixel technique (Helmer and Ruefenacht 2007). This method is based on two assumptions:

1. The atmospheric path radiance can be derived from the darkest water pixel of the satellite image due to the total light absorption and the radiation light recorded by the corresponding pixel.
2. The atmospheric path radiance is assumed to be uniform throughout the image. For each band, the darkest pixel can be determined from the lowest pixel values over water over the selected wavelength. The radiation of the darkest water pixel (assumed to represent the atmosphere) is subtracted from the entire image.

Radiometric calibration

When using multi-temporal satellite images, it is crucial to analyse abrupt changes in the vegetation cover, due to the lack of homogeneity of the time series of satellite images (Vicente-Serrano et al. 2008). This homogeneity is affected by noise from surface signals and the absorption and scattering by atmospheric gaseous and aerosol particles travelling through the atmosphere of the earth and back to the sensor (Janzen et al. 2006). The atmospheric effects may result in an improper interpretation of the satellite images (Tokola et al. 1999). Therefore, to analyse the change detection in vegetation density using a normalised difference vegetation index (NDVI), the atmospheric effect must be eliminated when pre-processing the satellite images (Song et al. 2001). In image classification, atmospheric correction and radiometric correction are not needed. Indeed, the atmospheric effects do not affect the output of the image after undergoing classification.

In radiometric calibration, a precise conversion of the digital number (DN) for Landsat ETM+ and TM to

satellite radiance unit (L) (Mather 2004; Vicente-Serrano et al. 2008; Chander et al. 2009a) is possible by using the following equation:

$$L_\lambda = \left(\frac{\mathrm{LMAX}_\lambda - \mathrm{LMIN}_\lambda}{Q_{\mathrm{calmax}} - Q_{\mathrm{calmin}}}\right)(Q_{\mathrm{cal}} - Q_{\mathrm{calmin}}) + \mathrm{LMIN}_\lambda \quad (1)$$

where L_λ spectral radiance at the sensor's aperture (W m^{-2} sr^{-1} μm^{-1}), LMAX_λ spectral radiance scaled to Q_{calmax} (W m^{-2} sr^{-1} μm^{-1}), LMIN_λ spectral radiance scaled to Q_{calmin} (W m^{-2} sr^{-1} μm^{-1}), Q_{calmax} maximum quantised calibrated pixel value (DN = 255) corresponding to LMAX_λ, Q_{calmin} minimum quantised calibrated pixel value (DN = 0) corresponding to LMIN_λ, Q_{cal} quantised calibrated pixel value [DN].

All of the constants were obtained from the study done by Chander et al. (2009b).

The value of radiance that was obtained was converted to top of the atmosphere (TOA) reflectance according to Chander et al. (2009b):

$$\rho = \frac{\pi L d^2}{\mathrm{ESun}_{\lambda \cos\theta}} \quad (2)$$

where ρ is the TOA reflectance for band λ, d the Earth–Sun distance in astronomical units, ESun_λ the mean solar-exoatmospheric irradiance for band λ, and θ is the solar zenith angle in degrees. ESun_λ values were obtained from Chander and Markham (2003) for the TM image and from the Landsat-7 Science Data User Handbook for the ETM+ image (http://ltpwww.gsfc.nasa.gov/IAS/handbook/handbook_toc.html). The use of the TOA reflectance eliminates the effect of differing solar zenith angles due to the different time and date of acquisitions. In addition, the TOA reflectance corrects for uncertainty in the Earth–Sun distance between differing dates of data acquisition. Therefore, when comparing different sensors, the TOA reflectance will give a more accurate result than the at-sensor spectral radiance.

Relative radiometric normalisation technique

Noise due to atmospheric effect exists due to the variation in reflectance for various types of vegetation. The conditions can worsen especially in a large coverage area used for multi-temporal satellite imagery (Xian et al. 2009). For change detection and monitoring applications, the factors of solar irradiance, atmospheric effects caused by absorption, and scattering, noise of the detector must be considered (Coppin et al. 2004). It is necessary to normalise all of these effects. Furthermore, in order to improve homogenous multi-temporal satellite images, one may perform a relative normalisation between two different satellite images, such as the relative radiometric normalised technique (Yuan and Elvidge 1996; Tokola et al. 1999; Lu et al. 2004; Nelson et al. 2005). The relative radiometric normalised technique is applied to find a linear relationship between two images in the form of DNs, radiance, TOA reflectance or surface reflectance values. When relative radiometric normalisation is performed, it is useful to detect and analyse the change detection for multi-temporal satellite images, such as NDVI. This is one of the atmospheric correction techniques used for satellite data (Janzen et al. 2006). In this relative radiometric normalisation technique, all of the images are adjusted to one reference image. The reference image is normally the most recent image and is the least affected by clouds or atmospheric effects. Through a linear regression analysis, the other images are normalised to the reference image for the reflectance values as follows (Vicente-Serrano et al. 2008):

$$\rho_{\mathrm{reference},\lambda} = a + b\rho_{\mathrm{normalised},\lambda} \quad (3)$$

where $\rho_{\mathrm{reference},\lambda}$ is the reflectance value for the reference image, $\rho_{\mathrm{normalised},\lambda}$ the subject image that is to be normalised, a the slope or gain and b is the intercept or offset.

The most tedious task encountered when applying the relative radiometric normalisationed technique is choosing suitable targets on the satellite images (Vicente-Serrano et al. 2008). Any mistake will affect the accuracy of the result, which will result in a poor correlation between two different images after regression. Uncertainty or misinterpretation is affected mainly by the noise of the sensor and the atmospheric effects. To complete the task, several criteria should be considered when choosing constant targets based on non-variance [pseudo-invariant features (PIF)], (Schott et al. 1988). Therefore, the following criteria should be taken into consideration:

1. Targets like water, asphalt and sand are usually selected as PIFs because their reflectances remain constant for a long time and are less affected by atmospheric effects.
2. Targets must be found in an area that has minimum vegetation coverage. The reflectance for vegetation may vary or change drastically within the time period of two multi-temporal satellite images.
3. If possible, targets with a wide range of reflectance values should be to be included (from bright to dark area).

In this study, the Landsat image, acquired on December 27, 1999 (Landsat 7 ETM+) was chosen as the reference image, and an image from February 8, 2007 was chosen as the normalised image. The reference image was previously atmospherically corrected (darkest pixel technique), while the normalised image was normalised to the reference image using a relative radiometric normalisation technique.

Image classification

Land cover as a basic parameter to evaluate the contents of the earth's surface is an important factor that affects the ecosystem's condition and function (Lunetta et al. 2006). Land cover, as a biophysical state of the earth can be used to estimate interactions in the forms of biodiversity, biosphere–atmospheric and geosphere–atmospheric interactions. In addition, multi-temporal maps of land use and land cover changes (LULC) are useful in identifying temporal changes, which have implications for local, regional or global environmental changes. Furthermore, abrupt changes in surface content may be due to the natural environment or anthropogenic activities (Fernandes et al. 2004). All of these may be interrelated.

The goal of the classification analysis is to categorise all of the pixels in the digital satellite images into land cover classes. Basically, the process can be divided into three simple steps: the pre-processing, data classification and output. For the first step of pre-processing, the digital satellite images were chosen for land cover mapping. For the second step of data classification, the digital satellite images were processed using the PCI Geomatica 10.1 software package. Supervised classifications operate in three basic steps: training, classification and accuracy assessment. Training sites are needed for supervised classification. The areas were established using polygons and were delineated by spectrally homogenous sub-areas, which have given class name. The satellite images were then classified using three supervised classification methods (maximum likelihood, minimum distance-to-mean and parallelepiped).

In this study area, seven LULC types were classified, including forest, grassland, urban (highly built-up areas), urban (minimally built-up areas), barren land, water and clouds. Supervised classification was undertaken for these two satellite images. Three measurements of accuracy assessment were carried out for each of the classification methods mentioned above, such as the overall accuracy, error matrix and Kappa coefficient. The error matrix is the term used to describe the measure of accuracy between the images that have been classified and the training side of the same image. It is widely used and comprises the core of the accuracy assessment literature (Foody 2002). A total of 200 random points were assessed for this study and the same vector layers of points were applied to both of the satellite images. A total of 100 training sample areas were selected for this analysis. For each scene, all seven bands in Landsat 7 ETM+ and Landsat 5 TM were used in the multi-spectral classification analysis, which use the previously mentioned classifiers. To improve the accuracy assessment between the classified areas and the training side, at least 20 points in the study area were identified regarding the classes, before undergoing supervised classification.

Land surface temperature retrieval

In order to obtain the impact of LULC on LST, LST data were retrieved from the radiometrically and geometrically corrected images using ATCOR3_T, using the PCI Geomatica version 10.1 digital image processing software. ATCOR3_T generates a surface thermal map using elevation data. It considers the slope and aspect images to produce an accurate retrieval of LST values over high mountain terrain. ATCOR3_T is useful to evaluate LST in 3D, because the digital elevation model (DEM) must be used to generate the LST map. Therefore, in this study, the reference DEM model known as the Shuttle Radar Topography Mission (SRTM) was used to retrieve the LST. The geometrically and radiometrically corrected SRTM satellite image was downloaded from the website of the global land cover facility. In addition, ATCOR3_T also has a built-in function for atmospheric correction, which is only available for band 6 (thermal band) Landsat data. The user must provide the input layer with specific visibility parameters (Richter 1990) to perform the atmospheric correction. The other input parameters required are the data acquisition and solar azimuth and solar zenith angles. All of these input parameters may be obtained from the header file of satellite imagery. For the visibility of satellite images obtained from Penang, Malaysia Forecast Weather Underground (http://www.wunderground.com/global/stations/48601/html) was used. The supported sensors that retrieved LST by ATCOR3_T are Landsat-4/5 TM (band 6), Landsat-7 ETM+ (band 6) and ASTER (band 13).

NDVI computation

With the recent improvements in remote sensing techniques, it is possible to obtain multi-temporal and multi-spectral remote sensing data, in order to provide an effective way to study the distribution of the vegetation index (Ding et al. 2007; Raynolds et al. 2008). The NDVI is usually used as a parameter to observe the spatial density distribution and growth status of a plant (Sun et al. 1998). This is because vegetation is very sensitive to the absorption and reflection of the red and infrared bands. Therefore, NDVI may be used as an indicator for the biomass and greenness of the earth's surface (Chen and Brutsaert 1998). Furthermore, NDVI has also been found to be a good indicator of surface radiant temperature (Lo et al. 1997). In this study, the relationship between LST and vegetation greenness (NDVI) was examined. NDVI values for both satellite images were calculated as the ratio between measured reflectance in the red (R) and near-infrared (NIR)

bands based on the following formula (Xiao and Weng 2007):

$$\mathrm{NDVI} = (\rho(\text{band 4}) - \rho(\text{band 3}))/(\rho(\text{band 4}) + \rho(\text{band 3})) \quad (4)$$

where, ρ is the surface reflectance for band 3 and band 4, respectively.

Usually, the index value of NDVI is in the range of −1 to 1. The higher the NDVI value, the denser and healthier the vegetation in that particular area. In terms of absorption, green vegetation is more sensitive to the red band as compared to the NIR band. Therefore, the reflectance of the NIR band is larger than that of the red band, which then gives a higher NDVI index. The normal healthy vegetation index falls between the ranges of 0.1–0.75, while for rock and soil, the NDVI values are close to zero, and water bodies give a negative reading for the NDVI value.

Cloud masking

One of the obstacles encountered in remote sensing with optical satellite imagery is persistent cloud cover (Helmer and Ruefenacht 2007). The mapping of a landscape in a tropical area for LULC changes is often restricted by the presence of cloud cover in the proposed study area. Cloud detection techniques are applied to mask the cloud-covered area and to let that area becomes null. There are few techniques available for cloud detection for satellite imagery. However, of all these techniques, two cloud detection tests have been carried out. These involve the ratio of NIR reflectance to visible reflectance and a gross cloud check using brightness temperature (Simpson and Gobat 1996). The gross cloud check that uses the brightness temperature technique is capable of detecting clouds for daytime or night-time scenes. However, this method is unable to detect warm low clouds above the sea. Therefore, the ratio of NIR reflectance to visible reflectance method was chosen to detect cloudy pixels above the study area. The ratio used in the test is defined as follows (Saunders and Kriebel 1988):

$$Q = \frac{R_2}{R_1} \quad (5)$$

where, Q is the ratio between R_2, NIR reflectance and R_1, visible reflectance.

The value of the brightness temperature is required to apply the gross cloud check technique. The at-sensor brightness temperature assumes that the earth' surface is a black body and includes atmospheric effects. The conversion of the brightness temperature from at-sensor radiance is given by Chander et al. (2009a, b)

$$T = \frac{K_2}{\mathrm{LN}\left[\frac{K_1}{L_\lambda} + 1\right]} \quad (6)$$

where T is the effective at-sensor brightness temperature (in Kelvin), K_2 is the calibration constant 2 (in Kelvin), K_1 is the calibration constant 1 (W m^{-2} sr^{-1} μm^{-1}), L_λ is the spectral radiance at the sensor's aperture (W m^{-2} sr^{-1} μm^{-1}), and LN is the natural logarithm.

Results and discussion

LULC changes and analysis in Penang Island, from 1999 to 2007

Figure 2a, b show the map after the classification of different LULC changes over Penang Island, for the year 1999 and 2007. The overall accuracy and Kappa coefficients for the LULC maps from 1999 to 2007 were compared using each of the classification methods: maximum likelihood classification, minimum distance-to-mean and parallelepiped (Table 1). Obviously, the maximum likelihood classification method gives the best result all of the methods. The overall accuracy and Kappa coefficient obtained using maximum likelihood classification for the LULC map for 1999 are 95.0% and 0.925. For the year 2007, the overall accuracy and kappa coefficient are 96.5% and 0.945. Tables 2 and 3 show the error matrix of the classified data and reference data for the satellite images from 1999 to 2007. In terms of the producer's accuracy (1999), all classes were >80% for the LULC map. The user's accuracies for all classes exceeded 80%. This implies that the classification was done with the highest accuracy. For the conditional Kappa statistics of each LULC class, all were >0.80 with the exception of the barren land. The barren land may have been confused with the grassland area in 1999. In the classification map of LULC in 2007, both the producer's accuracy and user's accuracy exceeded 85.0%, except for the barren land, which was only 66.67% for the user's accuracy. Furthermore, all classes also exhibited a Kappa statistic >0.85, but the barren land gave the lowest value, which was 0.663. The barren land and urban (highly built-up area) land showed significant confusion because both of these classes had quite similar values of reflectance. This caused the user to completely misclassify the areas containing barren land and urban (highly built-up area) land.

Table 4 shows the statistical analysis of LULC changes in Penang Island from 1999 to 2007. From this table, it is obvious that there has been a drastic change in urban areas (highly built-up areas), which increased 109.03% over the 8-year period. The area increased from 31.23 to 65.28 km^2

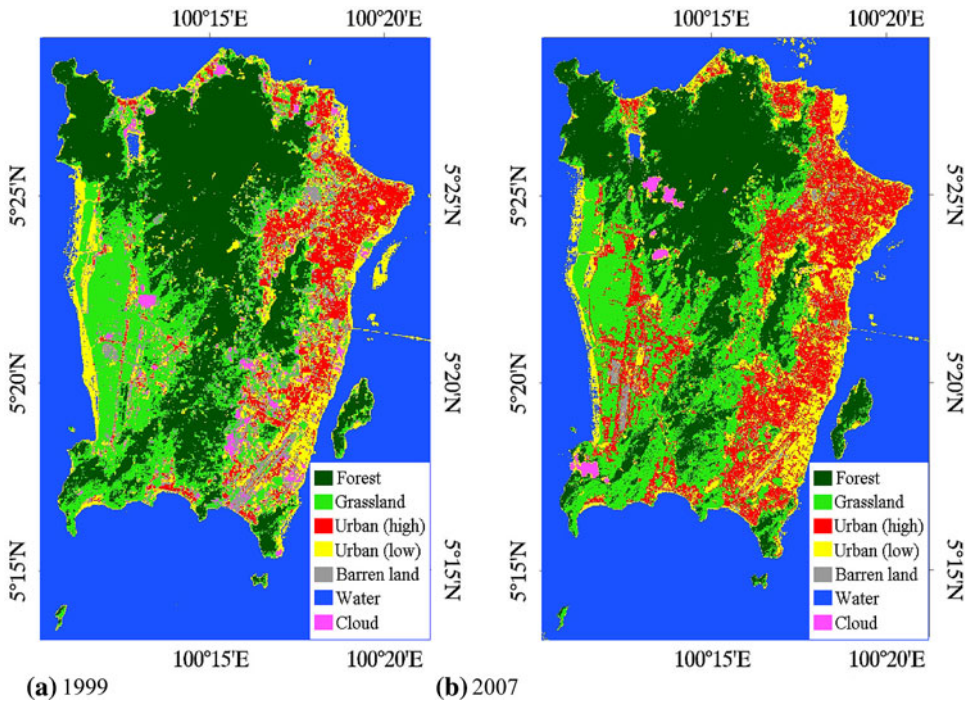

Fig. 2 Classification map for different LULC changes over Penang Island in 1999 (**a**) and 2007 (**b**) using the maximum likelihood classification method

Table 1 The overall classification accuracy and Kappa coefficient for the land cover map, 1999 and 2007

Classification method	Overall classification (%)		Kappa coefficient	
	1999	2007	1999	2007
Maximum likelihood	95.000	96.500	0.925	0.945
Minimum distance-to-mean	81.000	87.000	0.709	0.795
Parallelepiped	8.500	55.000	0.044	0.381

Table 2 Error matrix of the LULC map, 1999

Classified data	Reference data									
	FO	GR	UH	UL	BL	WA	CL	Total	UA (%)	κ_c, Kappa coefficient
FO	29	2	0	0	0	0	0	31	93.55	0.924
GR	1	23	1	1	1	0	0	27	85.18	0.829
UH	0	0	11	1	0	0	0	12	91.67	0.911
UL	0	1	0	16	0	0	0	17	94.12	0.935
BL	0	1	0	0	4	0	0	5	80.00	0.795
WA	0	0	0	1	0	105	0	106	99.06	0.980
CL	0	0	0	0	0	0	2	2	100.00	1.000
UC	0	0	0	0	0	0	0	0		
Total	30	27	12	19	5	105	2	200		
PA (%)	96.67	85.18	91.67	84.21	80.00	100.00	100.00			

FO forest, *GR* grassland, *UH* urban (highly built-up area), *UL* urban (minimally built-up area), *BL* barren land, *WA* water, *CL* cloud, *UC* unclassified, *PA* producer's accuracy, *UA* user's accuracy

during this period. On the contrary, barren land decreased obviously in this 8-year period by about 77.69% (from 23.85 to 5.32 km^2). Meanwhile, the forest area decreased moderately by around 16.89%. However, the grassland area increased during this period by nearly 12.67%. In addition, urban areas (minimally built-up areas) decreased

Table 3 Error matrix of the LULC map, 2007

Classified data	Reference data									
	FO	GR	UH	UL	BL	WA	CL	Total	UA (%)	κ_c, Kappa coefficient
FO	25	1	0	0	0	0	0	26	96.15	0.955
GR	2	26	1	0	0	0	0	29	89.65	0.880
UH	0	0	15	1	0	0	0	16	93.75	0.932
UL	0	1	0	10	0	0	0	11	90.91	0.904
BL	0	0	1	0	2	0	0	3	66.67	0.663
WA	0	0	0	0	0	113	0	113	100.00	1.000
CL	0	0	0	0	0	0	2	2	100.00	1.000
UC	0	0	0	0	0	0	0	0		
Total	27	28	17	11	2	113	2	200		
PA (%)	92.59	92.86	88.23	90.91	100.00	100.00	100.00			

FO forest, *GR* grassland, *UH* urban (highly built-up area), *UL* urban (minimally built-up area), *BL* barren land, *WA* water, *CL* cloud, *UC* unclassified, *PA* producer's accuracy, *UA* user's accuracy

Table 4 Statistical analysis for different LULC changes for 1999 and 2007

Classes	1999 (km^2) area	Percentage (%) of satellite image	2007 (km^2) area	Percentage (%) of satellite image
Forest	124.71	20.73	103.64	17.23
Grassland	74.27	12.35	83.68	13.91
Urban (highly built-up area)	31.23	5.19	65.28	10.85
Urban (minimally built-up area)	50.27	8.36	47.95	7.97
Barren land	23.85	3.97	5.32	0.88
Water	289.95	48.20	292.12	48.56
Cloud	7.24	1.20	3.53	0.59
Total	601.52	100.00	601.52	100.00

Table 5 Results of land use classification for 1999 and 2007 images showing area changes of each class

Classes	Area change from 1999 to 2007 (km^2)	Percentage (%)
Forest	−21.07	−16.89
Grassland	9.41	12.67
Urban (highly built-up area)	34.05	109.03
Urban (minimally built-up area)	−2.32	−4.61
Barren land	−18.53	−77.69
Water	2.17	0.75

slightly, by around 4.61%. In 1999, urban areas (minimally built-up areas) showed ground coverage of 50.27 km^2 and decreased to 47.95 km^2 in 2007. For the water area, the area increased slightly from 1999 to 2007, nearly 0.75%. Table 5 shows the detailed of area changes for each of the land cover classes from 1999 to 2007.

The most significant change is the expansion of urban areas (highly built-up areas) for the classification of LULC changes over Penang Island. Within a period of 8 years, the urban (highly built-up areas) land area increased by 109.03%. This means that for each year, the urban areas (highly built-up areas) increased by nearly 13.63%. If this trend continues for the following 8 years, in 2015, the urban areas (highly built-up areas) will most probably increase by about a factor of 2, as compared to 2007. In the late 1990s, the state government of Penang proposed and promoted a plan to make Penang state the state of "Tax-Free World Trade Centre". Many entrepreneurs around the

Table 6 Average land surface temperature (LST) in °C for different land covers

Land cover	1999	Standard deviation	2007	Standard deviation
Forest	29.43	1.12	28.78	0.85
Grassland	35.74	1.03	34.87	0.74
Urban (highly built-up area)	45.07	1.20	45.19	1.18
Urban (minimally built-up area)	39.22	1.89	40.45	2.23
Barren land	40.58	0.76	44.00	1.59

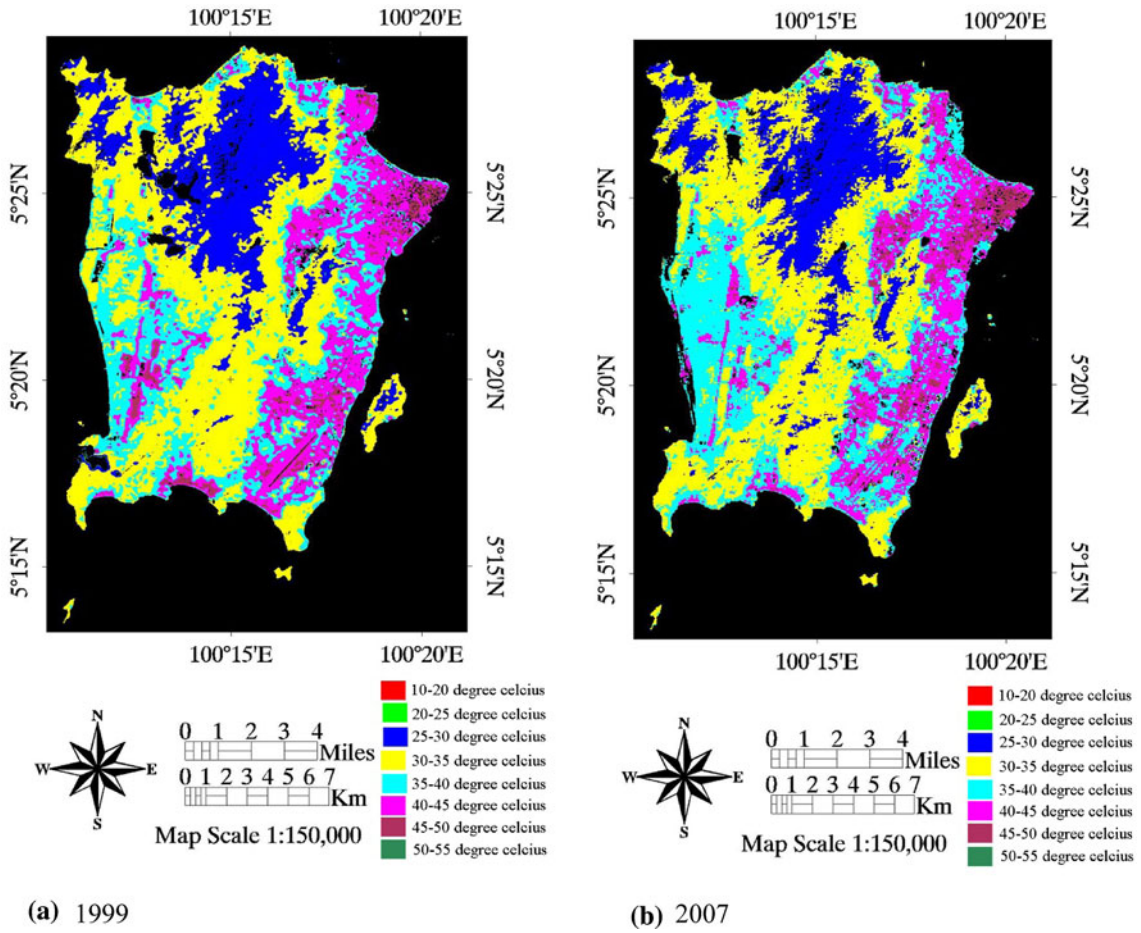

Fig. 3 The maps of LST retrieved using ATCOR3_T for 1999 (**a**) and 2007 (**b**), where *black colour* indicates water areas or cloud coverage and is null

Table 7 Linear regression correlation coefficients between LST in °C and NDVI by land cover types

Land cover	1999	R^2	2007	R^2
Forest	LST = −20.87NDVI + 43.389	0.810	LST = −14.78NDVI + 37.75	0.840
Grassland	LST = −2.3494NDVI + 35.427	0.595	LST = −7.3455NDVI + 38.227	0.775
Urban (highly built-up area)	LST = −16.216NDVI + 48.333	0.735	LST = −18.015NDVI + 47.776	0.757
Urban (minimally built-up area)	LST = −15.506NDVI + 42.14	0.661	LST = −16.252NDVI + 42.349	0.724
Barren land	LST = −6.9117NDVI + 39.564	0.463	LST = −10.445NDVI + 44.642	0.590

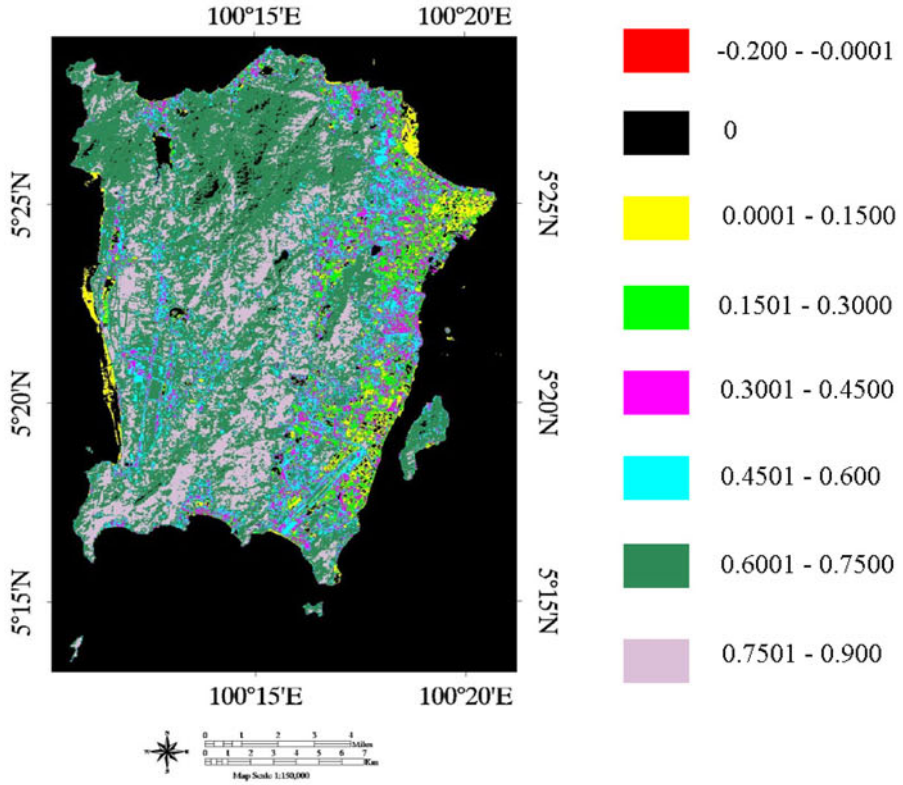

(a) 1999

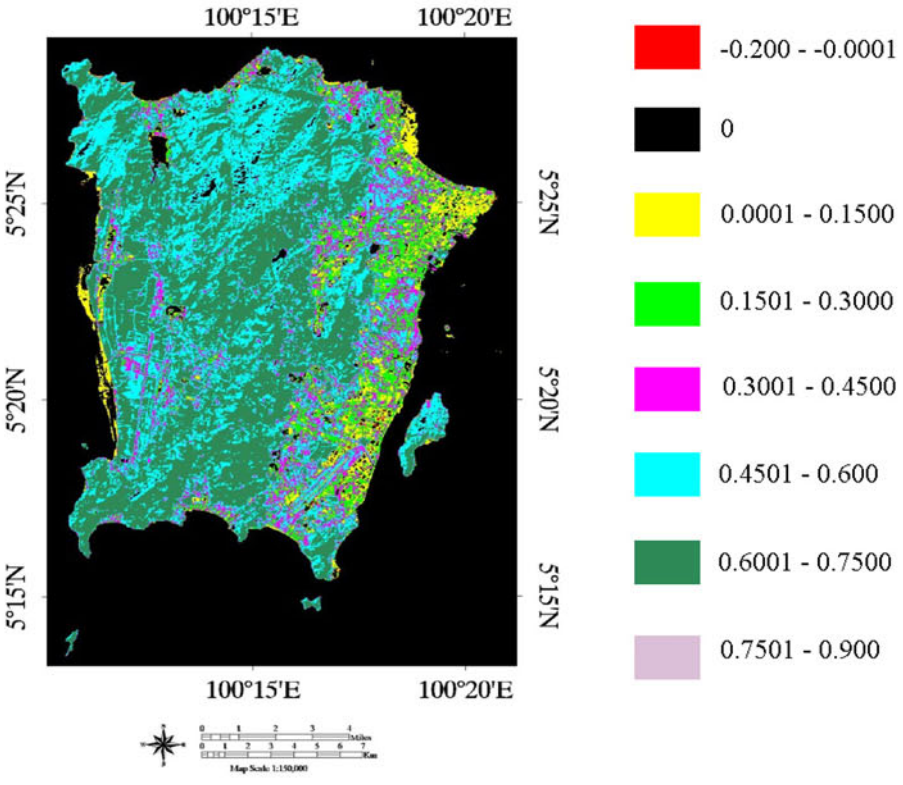

(b) 2007

Fig. 4 The maps generated based on NDVI computation for 1999 (**a**) and 2007 (**b**), using relative radiometric normalization. *Black colour* indicates water areas or cloud coverage

world have begun to invest in Penang Island. The attraction of investments caused Penang Island to change from a residential island to an industrial area. For example, Bayan Lepas has become the most notable place where many factories have been built. Indeed, Bayan Lepas also has an international airport. The airport connects the small island to many countries. In addition, it provides efficient transportation for imports and exports, which is suitable for worldwide trading. Furthermore, Penang Island has been a strategic place and has been well-known as a world trade centre since the early nineteenth century. In addition, the observed expansion of the urban area could be explained by the rapid increase of the urban population. Many people have begun to migrate from the rural villages to the city since the late of 1990s due to the rapid economic development.

Urbanisation impact on LST

Both satellite images have been studied for the characteristic of the surface temperature of each land cover type. This helps to more easily understand the impacts of LULC change on the LST. The average LST data for each land cover type in 1999 and 2007 are summarised in Table 6. It is obvious that for both 1999 and 2007, the urban type (highly built-up areas) exhibits the highest LST as compared to other land cover types (Weng 2001), (45.07°C in 1999 and 45.19°C in 2007), followed by barren land (40.58°C in 1999 and 44.0°C in 2007) (Fig. 3). In addition, the urban type (minimally built-up areas) also exhibits a high LST (39.22°C in 1999 and 40.45°C in 2007). This shows that urbanisation has caused an increase in LST since the modification of vegetation areas to impervious surface materials, such as concrete, tars, stone, etc. The standard deviation for all three of these classes of land covers is small; it was <5%, except for the urban land cover type (minimally built-up area), in 2007. The fact that the LST standard deviations are small for of all these land cover types indicates that the modification of land surface properties does not cause a large variation in LST due to the dryness of non-evaporative materials. The lowest LST was observed in the forest (Weng 2001), (29.43°C in 1999 and 28.78°C in 2007), followed by grassland (35.74 and 34.87°C in 2007). The forest has the lowest LST when compared to other land cover types, because the forest contains a variety of dense vegetation. The processes of photosynthesis and transpiration help to reduce the heat in that particular area. Penang Island experiences high annual relative humidity in the range of 70–90%. Therefore, the impacts of urbanisation did not result in a great deal of variety of LST in urban areas between 1999 and 2007. Indeed, the high relative humidity can transfer the heat from urbanisation efficiently and naturally.

Relationship between LST and NDVI

The relationship between LST and the NDVI was investigated for each land cover type. Table 7 shows linear regression correlations between these two elements. From the obtained result it is obvious that LST values tend to negatively correlate with NDVI values for all land cover types in both years. The highest negative correlation coefficient was found in forest (1999, 0.810 and 2007, 0.840), followed by urban (highly built-up area) (0.735) in 1999 and grassland (0.775) in 2007. In both years, urban (minimally built-up area) showed significant correlation with (0.661) in 1999 and (0.724) in 2007. In 1999, grassland exhibited low correlation as compared with the correlation for grassland in 2007, which was about 0.595. Nevertheless, urban (highly built-up area) in 2007 also experienced high correlation between LST and NDVI, nearly 0.757. An even lower correlation was also observed in barren land for both years (0.463 in 1999 and 0.590 in 2007) (Weng 2001). The strong negative correlation between LST and NDVI indicates that the higher the surface temperature, the lower the value of biomass within all these land covers types. Figure 4 shows the NDVI map, which was computed from the Eq. 4.

Conclusion

In this study, an integrated approach of remote sensing was used to determine land use changes in Penang Island for the period of 1999–2007. The results illustrated that Landsat multi-temporal image could provide an accurate map and give detailed descriptions of land cover change across the study area. The result obtained through LULC can be used as essential information for decision-making in land management and policy making. The results showed that during the period of 1999–2007, urban (highly built-up area) areas increased by 109.03%. Meanwhile, for urban (minimally built-up area), the areas decreased by 4.61% within this period. For barren land, the area also decreased by 77.69% due to the urbanisation impact. The forest area decreased continuously from 1999 to 2007, by about 16.89%, which was caused by deforestation for urban use. The grassland area increased by 12.67%, and the water area also increased slightly by nearly 0.75%.

In 1999, the average LST for urban (highly built-up area) was 45.07°C and rose to 45.19°C in 2007, with a standard deviation of <5%. However, the retrieved LST values may be higher than the actual values because the effect of surface roughness is not taken into account when retrieving the LST values (Weng 2001). In addition, LST is also influenced by the land surface structure, water content and chemical composition (Snyder et al. 1998). Cassels

et al. (1992a, b) mentioned that, in order to improve the results obtained from LST, the temperature of every part in the vegetation-ground system must be taken into consideration. Furthermore, the effects of different canopy structures may also affect surface temperature.

A simple atmospheric correction known as the darkest pixel technique was used in this study. It assumed that the atmospheric path radiance correlates to the darkest water pixel of the satellite image, due to the total radiation light recorded by the corresponding pixel. The lowest value, or the darkest water pixel, is subtracted from the original image to help to reduce the atmospheric effect. Essentially, atmospheric correction is not necessary for land cover classification. However, it is compulsory if the study involves the NDVI computation (Song et al. 2001). In further studies, the atmospheric correction scheme will consider water vapour, aerosol absorption and scattering to improve the results of the NDVI.

Acknowledgments The authors gratefully acknowledge the financial support from the Digital Elevation Models (DEMs) Studies For Air Quality Retrieval From Remote Sensing Data Grant, account number: 304/PFIZIK/638103 and Environmental Mapping Using Digital Camera Imagery Taken From Autopilot Aircraft Grant, account number: 305/PFIZIK/613606, with additional support from the USM-RU-PRGS Grant, account number: 1001/PFIZIK/831024. Extended thanks to USM technical staffs for their supports and cooperation.

References

Ahmad F, Yahaya AS, Farooqi MA (2006) Characterization and geotechnical properties of Penang residual soils with emphasis on landslides. Am J Environ Sci 2(4):121–128

Cassels V, Sobrino JA, Coll C (1992a) On the use of satellite thermal data for determining evapotranspiration in partially vegetated areas. Int J Remote Sens 13(14):2669–2682

Cassels V, Sobrino JA, Coll C (1992b) A physical model for interpreting the land surface temperature obtained by remote sensors over incomplete canopies. Remote Sens Environ 39:203–211

Chander G, Markham B (2003) Revised Landsat-5 TM radiometric calibration procedure and postcalibration dynamic ranges. IEEE Trans Geosci Remote Sens 41(11):2674–2677

Chander G, Markham BL, Helder DL (2009a) Summary of current radiometric calibration coefficients for Landsat MSS, TM, ETM+, and EO-1 ALI sensors. Remote Sens Environ 113:893–903

Chander G, Markham BL, Barsi JA (2009b) Revised landsat-5 thematic mapper radiometric calibration. IEEE Geosci Remote Sens Lett 4(3):490–494

Chen D, Brutsaert W (1998) Satellite-sensed distribution and spatial patterns of vegetation parameters over a tallgrass prairie. J Atmos Sci 55:1225–1238

Chen XL, Zhao HM, Li PX, Yin ZY (2006) Remote sensing image-based analysis of the relationship between urban heat island and land use/cover changes. Remote Sens Environ 104:133–146

Cohen W, Goward S (2004) Landsat's role in ecological applications of remote sensing. Bioscience 54:535–545

Coppin P, Jonckheere I, Nackerts K, Muys B (2004) Digital change detection methods in ecosystem monitoring: an review. Int J Remote Sens 25(9):1565–1596

Dash P, Gottsche FM, Olesen FM, Fischer H (2002) Land surface temperature and emissivity estimation from passive sensor data: theory and practice-current trends. Int J Remote Sens 23(13):2563–2594

Ding M, Zhang Y, Liu L, Zhang W, Wang Z, Bai W (2007) The relationship between NDVI and precipitation on the Tibetan Plateau. J Geogr Sci. doi:10.1007/s11442-007-0259-7

Fernandes R, Fraser R, Latifovic R, Cihlar J, Beaubien J, Du Y (2004) Approaches to fractional land cover and continuous field mapping: a comparative assessment over the BOREAS study region. Remote Sens Environ 89:234–251

Foody GM (2002) Status of land covers classification accuracy assessment. Remote Sens Environ 80:185–201

Han K-S, Viau AA, Anctil F (2004) An analysis of GOES and NOAA derived land surface temperature estimated over a boreal forest. Int J Remote Sens 25(21):4761–4780

Helmer EH, Ruefenacht B (2007) A comparison of radiometric normalization methods when filling cloud gaps in Landsat imagery. Can J Remote Sens 33(4):325–340

Houghton JT, Ding Y, Griggs DJ, Noguer M, van der Linden PJ, Dai X (2001) Climate change 2001: the scientific basis. Cambridge University Press, Cambridge

Janzen DT, Fredeen AL, Wheate RD (2006) Radiometric correction techniques and accuracy assessment for Landsat TM data in remote forested regions. Can J Remote Sens 32(5):330–340

Kabbara N, Benkhelil J, Awad M, Barale V (2008) Monitoring water quality in the coastal area of Tripoli (Lebanon) using high-resolution satellite data. ISPRS J Photogramm Remote Sens 63(5):488–495

Liu Y, Hiyama T, Yamaguchi Y (2006) Scaling of land surface temperature using satellite data: a case examination on ASTER and MODIS products over a heterogeneous terrain area. Remote Sens Environ 105:115–128

Lo CP, Quattrochi D, Luvall J (1997) Application of high resolution thermal infrared remote sensing and GIS to assess the urban heat island effect. Int J Remote Sens 18:287–304

Lu D, Mausel P, Brondizio E, Moran E (2004) Change detection techniques. Int J Remote Sens 25(12):2365–2407

Lunetta RS, Elvidge CD (1998) Remote sensing change detection: environment monitoring methods and applications. Taylor and Francis, London

Lunetta RS, Knight JF, Ediriwickrema J, Lyon JG, Worthy LD (2006) Land-cover change detection using multi-temporal MODIS NDVI data. Remote Sens Environ 105:142–154

Mallick J, Kant Y, Bharath BD (2008) Estimation of land surface temperature over Delhi using Landsat and ETM+. J Indian Geophys Union 12(3):131–140

Mather PM (2004) Computer processing of remotely-sensed images—an introduction, 3rd edn. Wiley, New York, p 134

Nelson T, Wilson HG, Boots B, Wulder MA (2005) Use of ordinal conversion for radiometric normalization and change detection. Int J Remote Sens 26(3):535–541

Qin Z, Karnieli A (1999) Progress in the remote sensing of land surface temperature and ground emissivity using NOAA-AVHRR data. Int J Remote Sens 20(12):2367–2393

Raynolds MK, Comiso JC, Walker DA, Verbyla D (2008) Relationship between satellite-derived land surface temperatures, arctic vegetation types, and NDVI. Remote Sens Environ 112:1884–1894

Richter R (1990) A fast atmospheric correction algorithm applied to Landsat TM images. Int J Remote Sens 11(11):159–166

Saunders RW, Kriebel KT (1988) An improved method for detecting clear sky and cloudy radiances from AVHRR data. Int J Remote Sens 9:123–150

Schott JR, Salvaggio C, Volchok WJ (1988) Radiometric scene normalization using pseudoinvariant features. Remote Sens Environ 26:1–16

Schroeder TA, Cohen WB, Song C, Canty MJ, Yang Z (2006) Radiometric correction of multi-temporal Landsat data for characterization of early successional forest patterns in western Oregon. Remote Sens Environ 103:16–26

Simpson JJ, Gobat JI (1996) Improved cloud detection for daytime AVHRR sense over land. Remote Sens Environ 55:21–49

Snyder WC, Wan Z, Zhang Y, Feng YZ (1998) Classification-based emissivity for land surface temperature measurement from space. Int J Remote Sens 19(14):2753–2774

Song C, Woodcock CE, Seto KC, Lenney MP, Macomber SA (2001) Classification and change detection using Landsat TM data: when and how to correct atmospheric effects? Remote Sens Environ 75:230–244

Sun H, Wang C, Niu Z (1998) Analysis of the vegetation cover change and the relationship between NDVI and environment factors by using NOAA time series data. J Remote Sens 2(3):205–210

Sun Z, Ma R, Wang Y (2008) Using Landsat data to determine land use changes in Datong basin, China. J Environ Geol. doi: 10.1007/s00254-008-1470-2

Synder WC, Wan Z, Zhang Y, Feng YZ (1997) Requirement for satellite land surface temperature validation using a split playa. Remote Sens Environ 61:279–289

Tokola T, Lofman S, Erkkila A (1999) Relative calibration of multitemporal landsat data for forest cover change detection. Remote Sens Environ 68:1–11

Vicente-Serrano SM, Perez-Cabello F, Lasanta T (2008) Assessment of radiometric correction techniques in analyzing vegetation variability and change using time series of Landsat images. Remote Sens Environ 112:3916–3934

Weng Q (2001) A remote sensing-GIS evaluation of urban expansion and its impact on surface temperature in the Zhujiang Delta, China. Int J Remote Sens 22(22):1999–2014

Weng Q, Lo CP (2001) Spatial analysis of urban growth impacts on vegetative greenness with Landsat TM data. Geocarto Int 16(4):17–25

Xian G, Homer C, Fry J (2009) Updating the 2001 National Land Cover Database land cover classification to 2006 by using Landsat imagery change detection methods. Remote Sens Environ 113:1133–1147

Xiao H, Weng Q (2007) The impact of land use and land cover changes on land surface temperature in a karst area of China. J Environ Manag 85:245–257

Yuan D, Elvidge CD (1996) Comparison of relative radiometric normalization techniques. ISPRS J Photogramm Remote Sens 51:117–126